Predictive sensitivity analysis of motor's windings HF impedances

Arthur Piat, François Costa, Sami Hlioui, Pierre-Etienne Lévy

Predictive sensitivity analysis of motor's windings HF impedances

Arthur Piat[1,2]
[1]IRT Saint Exupéry Toulouse, France
[2]SATIE, Université Paris-Saclay, ENS Paris-Saclay , CNRS,
91190 Gif sur Yvette, France
arthur.piat@irt-saintexupery.com

Sami Hlioui[3]
[2]SATIE, CY Cergy Paris University, Université Paris-Saclay, ENS Paris-Saclay , CNRS,
91190 Gif sur Yvette, France
sami.hlioui@ens-paris-saclay.fr

Pierre-Etienne Lévy[2]
[2]SATIE, Université Paris-Saclay, ENS Paris-Saclay , CNRS,
91190 Gif sur Yvette, France
pierre-etienne.levy@ens-paris-saclay.fr

François Costa[4]
[4]SATIE, Université Paris Est Créteil, Université Paris-Saclay, ENS Paris-Saclay, CNRS,
91190 Gif sur Yvette, France
francois.costa@ens-paris-saclay.fr

***Abstract*—This paper describes a process in which high frequency (HF) differential-mode (DM) and common-mode (CM) impedances of a Permanent Magnet Synchronous Motor (PMSM) are predicted. These tools, using both 2D Finite Element Modeling (FEM) and Spice lumped parameter circuit, are then used to generate sensibilities analysis such as Sobol and Correlation indices with the help of surrogate models. This method gives a better understanding of design choices that can be made to impact impedances values at both low and high frequency for a same load working point. Obtained simulation results are compared to experimental ones using statistics, showing the interest of such an approach.**

Keywords— Electromagnetic Compatibility (EMC), common-mode (CM), differential-mode (DM), electrical machine, HF modeling, finite element method, Sobol indices, Surrogate models

I. INTRODUCTION

Driven by the need to improve efficiency regarding environmental regulations and to open to new market segments, the need to embed electrical in aircraft is increasing against currently used systems driven by hydraulic or pneumatic energies [1]. A key solution may reside in emerging Wide-band gap semiconductors, namely SiC and GaN, increasing both efficiency and maximal power rating of embedded systems [2]. These achievements are performed using faster switching frequencies than conventional semiconductors, resulting in an increased spectrum of Electromagnetic Interferences (EMI) [3]. As perturbations will propagate in all possible path, numerous studies focused on measurement-based approaches [4]-[8]. Furthermore, theses interferences may reach neighboring systems and disturb their intended behavior [9]. To prevent such issues, various regulations limit the level of maximal authorized emissions [10].

Existing electrical power trains can be measured to extract behavioral models, allowing to numerically size filtering devices to reduce perturbations [11]-[14], but these approaches are bound to one existing system. Predictive modeling of perturbations generated by inverters [15] and transmission in lines such as cables [3], [16] are covered. Similar methods were then applied to electrical machines to predict the response to perturbations on a broad spectrum of frequency, few kHz to 10 MHz [14], [17]-[20] on both DM and CM or with the aim to predict overvoltage within stator windings and prevent partial discharge [21]-[23]. On another scope, the evaluation of CM capacitance due to probability density function was studied and demonstrated to have a significant impact on HF spectrum [24]. However, the impact of wire in parallel and their relative placement to each other's is yet to be quantified. Tendencies on various design variables exist [18], [19] but are not yet able to quantify those variations with regard to design variables, meanwhile impact of uncertainties are yet to be studied to authors' knowledge. This paper aims to provide an approach to determine the key design variables in low and high frequency for an electrical machine, given a fixed working point.

II. WINDING MODELING UNDER DESIGN PARAMETERS

To evaluate the impact on CM and DM impedances of design parameters, a similar simulation procedure to [18]-[19] is proposed: FEM models are used to extract impedance matrices, which are then used in a Spice environment to replicate the motor winding. Specific simulations are then evaluated to replicate impedance characterization performed on electrical machines. An overview of design variables is given in Table I.

TABLE I. DESIGN VARIABLES FOR EMC PMSM STUDY

Variables	*Description*
Tooth width	Width of the iron composing the motor tooth
Wires in hand	Number of wires used in parallel for each turn
Insulating paper	Paper thickness between wires and the iron stack
Slot permittivity	Relative permittivity filling the slot
Insulation percent	Enamel percentage following IEC 60317-13 (grades 1 to 3)

Numerous variables are necessary to describe the PMSM geometry but will not be studied here as the working profile of the motor is fixed. A key feature of this work is, however,

This paper is part of the OCEANE Project led by IRT Saint Exupéry, Toulouse (France), which is sponsored by AIRBUS, LIEBHERR, SAFRAN and the French National Research Agency (ANR) in collaboration with SATIE, TUD, DEEP, ICAM and LAPLACE.

to be able to evaluate the impact of different windings on HF impedances.

A. *Wire number and association*

For a given working point, a similar motor can be designed using different wires. Using wires in parallel, it may be possible to wound stators more easily than with a single and therefore more rigid wire, as well as reducing losses due to skin effect [25]. Thermal constraints are supposed similar if the overall copper surface by turn is kept, and more generally, considering that all parallel wires have the same impedance at every frequency.

B. *Order and position of wire groups in slots*

In a stator slot or wound rotor, the position of turns (groups of wire in parallel) in a slot is heavily dependent on the manufacturing process, and this order can have significant consequences on partial discharge and voltage levels between turns [21]-[23]. The impact on CM and DM impedances are yet to be quantified.

To consider the change in wires arrangement induced by the modified number of wires in parallel and the need to define groups, a protocol was developed, allowing filling any slot with any number of conductors and to group them into the needed number to fit the design parameter "Wire in hand" from Table I. In this paper, only arranged wire patterns are used, misplacement and intrusion of wires external of the given group were studied but is not the subject of this paper. Fig. 1a. features an example of an arranged winding with four wires in parallel in which all groups are assembled with the closest possible wires. The turns are also ordered so as the first turn is at the top of the slot, and all other turns are determined according to the relative position towards the first group. Fig. 1b shows an example of multiple insertions, not covered in this paper.

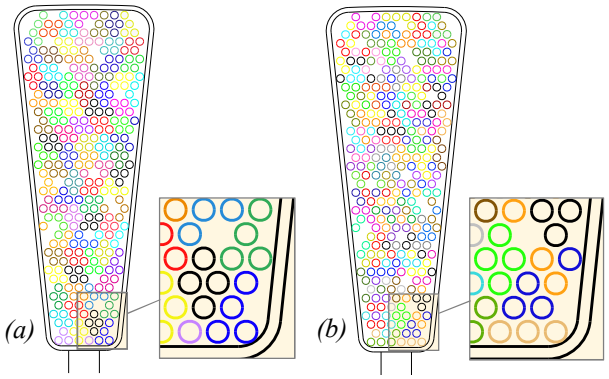

Fig. 1. Arranged winding (a) and winding with group intrusion (b) showing colored wires wound in parallel, for an 80-turn coil, 4 wires in parallel.

This process, while allowing generating windings for any number of wires in parallel and any size of wire, comes with some assumptions: wires are perfectly placed following and the hexagonal pattern evenly fill the slot, which is different from observed filling patterns [24]. In the case of a combination of wire diameter and wire number not allowing for a specific winding to be inserted within the slot space, the configuration is rejected and considered as infeasible. Once a configuration is determined feasible and all conductors placed and grouped, FEM simulation starts.

III. FEM SIMULATION AND MATRIX EXTRACTION

Four FEM models are generated for one slot configuration, two magnetic models to extract inductive and resistive phenomena and two electrostatic ones to compute capacitance matrices for all the wires, both in air and in the motor slot.

A. *PMSM slot modeling.*

With regard to the global design of the motor, the iron stack is supposed constant along the rotating axis of the rotor; therefore, a plane model was selected. Wires from the same group (meaning wires wound in parallel) are put to 1 A or 1 V to simulate respectively magnetic and electrostatic phenomena. FEMM [26] was used to extract magnetic impedances in the form of complex frequency dependent matrices, and a capacitance matrix, supposed fixed in frequency. In the specific case of electrostatic simulations, the slot surface is also fixed to the reference potential.

B. *PMSM end-winding modeling*

Similarly to their slot counterparts, two models will be used for end-windings, using not plane models but axisymmetric ones. It is supposed that coils produce perfectly shaped half circles between two slots and interactions with other coils, iron stacks and overall casing of the system can be neglected.

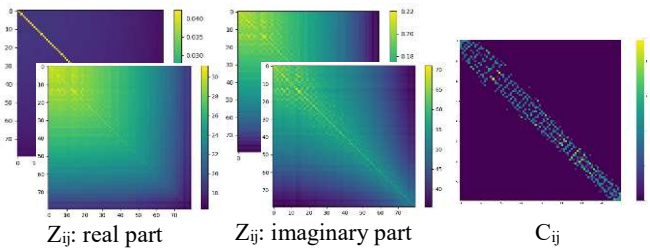

Fig. 2. Frequency dependent impedance and capacitance matrices for Fig. 1. (a) configuration

Fig. 2 features the real and imaginary parts of the magnetic impedance matrices noted Z_{ij}, at 1 kHz on the background, and 3.2 MHz on the front for the configuration displayed Fig. 1a, while capacitance matrix C_{ij} is shown on the right. For a PMSM with n-turn coils for instance, output data are of size n×n. These matrices are then used to generate Spice netlists for lumped parameter circuit simulations. For the magnetic simulation, the diagonal represents the self-resistance and inductance of all wires and capacities between wires and the slot surface of electrostatic simulations. The remaining parts represent coupling magnetic factors and inter-turn capacitances, similarly to [18], [19]. In the case of magnetics simulations, the mesh is refined as the frequency increases to ensure a mesh size inferior to the skin effect, allowing the extraction of values conservative of such phenomenon. This process generates important simulation times as the frequency increases. Therefore, simulations will be performed between 1 kHz and 10 MHz.

IV. SPICE TRANSLATION OF FEM MATRICES

All matrices computed using FEM are integrated in a Spice netlist in the form of lumped parameters. The goal is to replicate a unique coil of our motor which can be assembled

in series and parallel in a later study to be compared to working prototypes.

A. *Self inductances and resistances*

Resistances and self-inductances are derived from the real part of magnetic matrices Z_{ij}, these values are computed for each turn and consequently represent a unique or few conductors in parallels, relatively to the studied configuration, using the following equations:

$$R_{ii} = real(Z_{ii}) \quad (1)$$

$$L_{ii} = imag(Z_{ii})/w \quad (2)$$

B. *Coupled inductances and proximity effects*

Coupled inductances can be implemented in Spice netlist using coupling factor k which are computed using self and mutual inductance values:

$$k_{ij} = M_{ij} / \sqrt{L_{jj} . L_{ii}} \quad (3)$$

As featured in Fig. 2., the real part of the inductance matrices Z_{ij} are non-diagonal at high frequency. However, there is no component in Spice format which can represent such phenomena. In [14], those values were ignored but [18][19] showed a significant improvement in low frequency damping by integrating such values. This concept of "mutual resistance" have often been studied in transformers [27] and convey the loss generated by the inter-winding skin and proximity effects. Using behavioral voltage sources, these elements can be simulated with the following equation:

$$V_i = \sum I_j . R_{ij} \ , \forall i \neq j \quad (4)$$

Equation (4) features these mutual resistances and current flowing through other groups. The resulting voltage source is placed in series with self-inductances and resistances for a given group. This way of implementing all matrices is not unique and other methods exist [18][19].

C. *Interturns and wire to slot capacitances*

Capacitances are straightforward and can be inserted into the Spice netlist, wire to slot capacitances is placed between each turn and the ground, while inter-turns are places between each turn composing the coil as illustrated on Fig. 3.

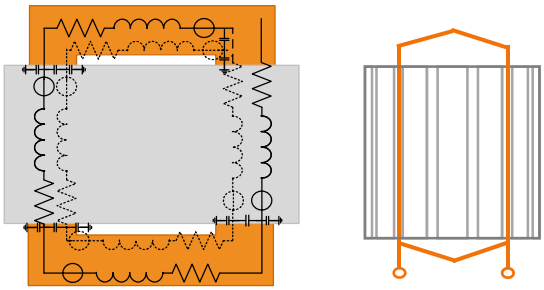

Fig. 3. Spice circuit of a simulated coil with matching simplified cross-sectional view

In the specific motor studied here, end-winding are of similar size as the iron stack therefore could not be neglected. As the values of inductances, resistances, coupling coefficient and behavioral voltage source vary in frequency, the Spice netlist is updated for each frequency simulated. One circuit is simulated in two configurations: one CM performed between the entry of the coil and the ground, and one DM between the entry and the end of the coil. Extracted impedances can be compared with measurements on prototypes.

V. Impedance Curves and Quantification of Variation

A sample of simulations performed using different values for "Wires in hand" from Table I. are shown in Fig. 4., respectively one for S1, four for S2 and sixteen for S3. There is a clear evidence of the impact of wires in parallel on the CM impedance, at every frequency

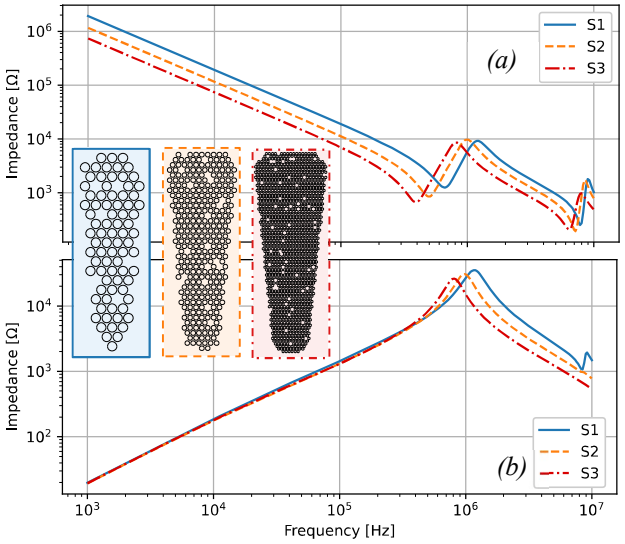

Fig. 4. (a) CM impedance and (b) DM impedance for an eighty turn coil using various wires in parallel.

Meanwhile, the DM impedance is very similar at low frequency but passed the first resonance, the behavior is very similar to the common mode impedance. This representation was used in many articles [17]-[20] and allows for a better understanding of the key factor changing the impedance on a wide band of frequency. However, it only gives tendencies and does not give how much the output (impedance curves) will vary based on the inputs interval. This is with these aspects in mind that another approach in shown in part VI

VI. Sensibility Analysis using Sobol Indices.

Sobol indices [28] are powerful tools to link the variation of an output parameter to the input, provided its design interval and probability presence within this interval. However, it requires a large number of experiments to be computed [28]. The overall simulation time being a key obstacle to the extensive simulations needed by such methodology, Sobol indices will be computed at few selected frequencies: 32 kHz and 2 MHz in this abstract for both CM and DM impedances as they were less inclined to present resonances. Moreover, a surrogate model was created from a Design Of Experiment (DOE) computed using Latin Hypercube Sampling with simulated annealing using Table I variables. Intervals for design variables are given in Table II column "I. With the help of a Gaussian Process Regressor (GPR) [29] algorithm, the data can be fitted and predicted accurately as shown in Table IV on a validation batch of 100 samples while 511 were used for training. The overall process of simulation, storing data, metamodeling and computation of Sobol indices was performed using GEMSEO [30].

TABLE II. DESIGN INTERVAL FOR EMC SENSIBILITY ANALYSIS

Variables	*Notation*	*Interval*	*Interval Sobol*
Tooth width	W_T	± 0.3 mm	± 0.15 mm
Wires in hand	N_w	n ∈ [1,5], n ∈ ℕ	n ∈ [1,4], n ∈ ℕ
Insulating paper	W_p	[0.1, 1.0] mm	[0.1, 0.51] mm
Slot permittivity	ε_s	ε_r =[1, 3]	ε_r =1
Insulation percent	$I_{\%}$	[0.69, 1.39] 0.69 ⇒grade 1, 1 ⇒ grade 2, 1.39 ⇒ grade 3	[0.69, 1.39]

TABLE III. MEAN VALUE AND STANDARD DEVIATION IN DOE

Output variable		*Deviation measurements*		
		Mean	*STD*	*STD/Mean*
Z_{DM}	32 kHz	555 Ω	18.2 Ω	3.28 %
	2 MHz	1077 Ω	502 Ω	46.6 %
Z_{CM}	32 kHz	29701 Ω	7915 Ω	26.6 %
	2 MHz	733 Ω	222 Ω	30.4 %
C_{CM}		$8.889 *10^{-11}$ F	$2.314 *10^{-11}$ F	26.0 %

TABLE IV. QUALITY MEASUREMENTS FOR GPR SURROGATE MODEL

Output variable		*Quality measurements*	
		R^2	*RMSE*[a]
Z_{DM}	32 kHz	0.6082	9.9831
	2 MHz	0.8580	$1.7415 *10^{2}$
Z_{CM}	32 kHz	0.9893	$7.9732 *10^{2}$
	2 MHz	0.9083	$6.6314 *10^{1}$
C_{CM}		0.9904	$2.0897 *10^{-12}$

[a] Root Mean Square Error

Z_{DM} and Z_{CM} represent the impedances computed using Spice, while C_{CM} is directly extracted from FEM simulations. This surrogate model is then used to generate a significant amount of data to compute Sobol indices. All variables from Table I are uniformly distributed to generate relevant Sobol indices as to match experimental validation, section VII (see Table II, column "Interval Sobol"). Table III gives the mean and standard deviations of outputs with performed DOE using Table II "Interval" column, showing the minor impact of all variables on Z_{DM} at 32 kHz, while featuring significant modification to C_{CM}, Z_{CM} (32 kHz, 2 MHz) and 2 MHz Z_{DM}.

A. Variability of Z_{CM} with regard to design interval

The Sobol indices' diagram of C_{CM} capacitance, using only FEM simulations, is very similar to Z_{CM} obtained with the Spice model as shown by Fig. 5., comforting the idea that low frequency capacitance is driven by the sum of all wire capacitance to the slot [3][8][17]-[20][24]. The standard deviation from Table III for Z_{CM} (32 kHz and 2 MHz) can be attributed to the number of wires in hand (N_W). The higher the frequency, the greater the impact of the enamel size ($I_{\%}$) increases due to turn-to-turn capacitance, the smaller the insulating paper width becomes. The enamel size is driven by the wire diameter, as it was determined that the average enamel width follows the rule:

$$W_e = (\emptyset_{wire} \times a + b) I_{\%} \qquad (5)$$

W_e being the enamel width, $\emptyset_{wire}$ the wire diameter and I_p the insulation percent. Both coefficient b and a being positive, the smaller the conductors are, the more enamel is present within the slot. Note that $I_{\%}$ allows testing between grade 1 and grade 3; therefore a sensibility analysis can be performed more easily using this continuous variable rather than a discrete one. The importance of the enamel size at high frequency is linked to inter-turn capacitances that plays a significant role on the CM impedance at higher frequencies [19][31] exceeding the variation created by the insulating paper. The number of wires in hand is also directly linked to the overall proximity of the copper surface to the slot as smaller wires will form a more compact layer around the slot (see Fig. 4a) resulting in a significant impact on the impedance at 32 kHz.

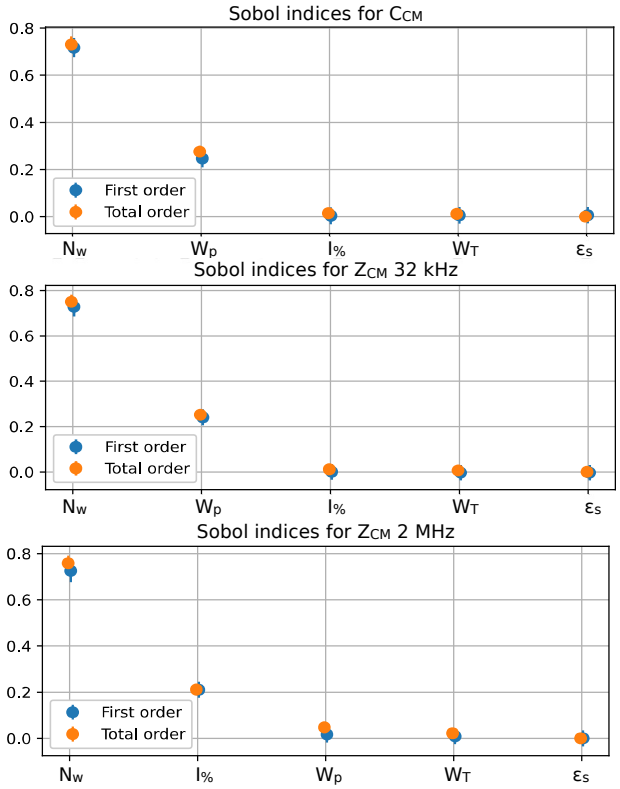

Fig. 5. Sobol indices for CM capacitance and CM impedances at 32 kHz and 2 MHz

The slot permittivity (ε_s), representing an overall impregnation of wire within the slot and the tooth size are, however, not impactful on the CM impedance, the reason is linked to the interval used for these simulations that are very limited (see Table II). Larger design intervals allow evaluating in more depth the various interactions between variables and their impact on the impedance but will not be studied in this paper.

B. Variability of Z_{DM} with regard to design interval

Sobol diagrams for Z_{DM} are shown in Fig. 6, featuring the same design variables as Z_{CM}. The diagram at 32 kHz places N_w as the most impactful variable. The variance is, however, very limited as seen on Fig. 4b and confirmed by Table III with a standard deviation limited to 3.2% for the mean value, linked to the appearance of skin effect in the case of a single wire per turn compared to other configurations. The Sobol diagram for 2 MHz is closer to the 2 MHz Z_{CM} diagram as the DM impedance follows a capacitive behavior at this frequency. With current design intervals, the number of wires in parallel remains the variable generating the most variation on the impedance, but variables linked to enamel size become more impactful as the frequency increases. To summarize, CM impedance is highly impacted by both the winding, the insulation parameters and the slot surface overall, meaning the working point and the overall choice in enamel in impregnation of the slot are decisive to the final value of impedances. Major care in the choice of enamel and impregnation material would allow keeping the CM

impedance within controlled margins. DM impedances are not extensively impacted by the variables studied at low frequency. However, the behavior at high frequency is very similar to the CM impedance and needs to be further studied to conclude on the source of all variations.

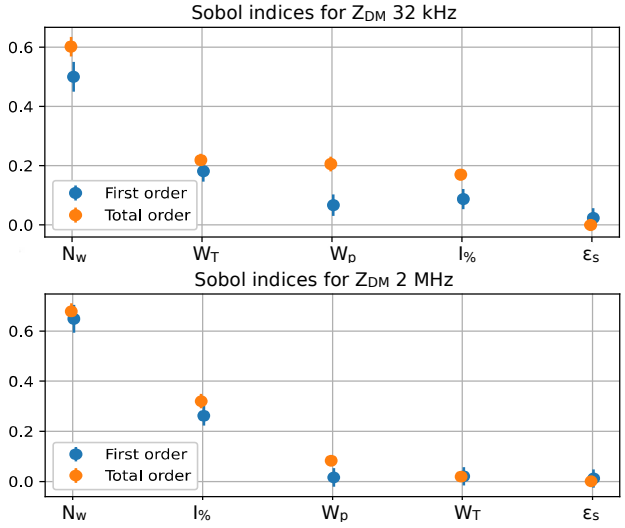

Fig. 6. Sobol indices for DM impedances at 32 kHz and 2 MHz

VII. Experimental Validation

Validating such approach is tedious; five hundred configurations can be simulated but creating this many prototypes to compare the result is very challenging. To validate such approaches, a simplified version of this problem was considered: three non-functional stators were assembled with three groups of three similar coils. Each prototype only has one variable changing between coil groups. Configuration 1 (noted C1 in Table V) changes the paper insulation width (0.1, 0.3 and 0.51 mm) Configuration 2 (C2) changes the number of wires in parallel (1, 4 and 16) while keeping the copper surface similar and finally Configuration 3 (C3) study enamel grades (grade 1, 2 and 3). The three prototypes were assembled to perform replicable measurements and have a connection to iron sheets as reference, shown on Fig. 7.

Fig. 7. Close-up look and global design for validation prototypes

All frequency measurements were performed using an impedance analyzer. Mean, STD and their ratio are computed while the surrogate model is used to match a sample with increased evaluations. Each coil is measured between 20 Hz and 120 MHz and all are used to generate a statistical evaluation of both impedances at 32 kHz and 2 MHz. Similarly to Table III, Table V features the ratio of STD divided by the mean value, giving the impact of variables on the different impedances but comparing these values to simulations.

TABLE V. STD/MEAN IN PERCENTAGE , MEASUREMENTS AND SIMULATION

configuration	Z_{DM} *32 kHz*	Z_{DM} *2 MHz*	Z_{CM} *32 kHz*	Z_{CM} *2 MHz*
	Measurements | *Simulation* *[%]*			
C1	3.01 | 1.62	27.6 | 21.8	6.38 | 8.54	7.59 | 4.83
C2	8.86 | 2.63	55.3 | 36.9	15.7 | 14.0	15.0 | 24.7
C3	2.71 | 1.76	14.4 | 27.4	9.77 | 1.27	14.7 | 18.4

On every frequency, both measurements and simulation give the maximal variation as the consequence of changing the number of wires in parallel. This matches all Sobol indices indicating the importance of such design variable on impedance for this design space, especially at HF. The enamel size also generates more variation as the frequency increase and is less impactful than the number of wires, on both Sobol indices and Table V statistics, one more aspect confirmed by measurements. The insulation paper width is very impactful on CM impedance at low frequency but its effect at high frequency is limited and significantly lower than the two other variables, shown by both Sobol and Table V. Meanwhile on the DM impedance, the simulation and Sobol feature a reduced importance of this parameter, on measurements it appears to be the second most important. The enamel size is indeed less impactful on DM measurements than simulations.

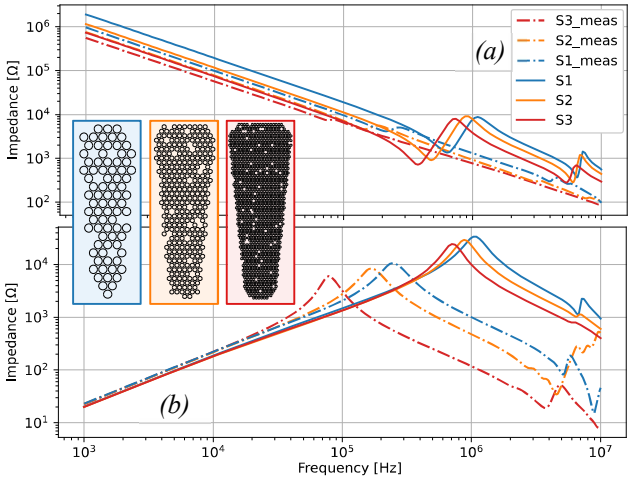

Fig. 8. (a) CM impedance and (b) DM impedance for stator configuration 2 measurements and simulations

This is supposedly linked to conductors' placement, minimizing inter-turn and wire to slot capacitance, changing the impact of such variables at higher frequency, compared to the model used. Conductors are forced into the slot and form a pattern with places with high and low-density areas [24]; meanwhile our simulations maximize the spaces between conductors. This difference may also explain the result on Z_{cm} 32 kHz, having very little differences between simulations due to similar placement (see S2 on Fig. 8). Indeed, as demonstrated in [31], a difference in wire to slot capacitance shift downward CM impedance curves and lower the frequency of CM and DM first resonance. The same goes for the inter-turn one but only after the first resonance. Consequently, a large difference between simulations and measurements can be seen in Fig. 8 with, however, tendencies correctly highlighted. Representing faithfully the mechanical placement of conductors appears to be the key to improving Sobol accuracy and predict the changes induced by design choices on a large spectrum of frequency.

VIII. CONCLUSION

In this paper, a methodology allowing for both CM and DM impedance predictions was presented combining FEM and Spice lumped parameter circuit. This allows representing impedances on a spectrum covering 1 kHz up to 10 MHz. The overall process was then used to generate a DOE with five variables of interest in order to train a surrogate model based on Gaussian Regressor Process to predict the impedance at two different frequencies. Sobol indices were then computed thanks to the reduced simulation time induced by the use of a surrogate model, compared to the initial simulation process. Sobol indices, linking output variations to inputs, give numerical quantification to which design variables are affecting the frequency response, both in CM and DM. This major result, allowing a designer to choose variables of interest to affect PMSM's HF impedance at a similar working point, was validated on prototypes representative of the system real design space. Although difference remains, impedance variation was linked to key design choices and identified main factors within the studied design space. Further work is needed to represent more faithfully higher frequency and validate such results on a larger sample size. These aspects will be the focus of later research.

REFERENCES

[1] R. Berger, M. Nazukin, N. Sachdeva and N. Martinez, "Think: Act Aircraft Electrical Propulsion - The Next Chapter of Aviation ?" Roland Berger LTD, 2017

[2] H. H. Sathler, "Optimization of GaN-based Series-Parallel Multilevel Three-Phase Inverter for Aircraft applications". PhD dissertation. Université Paris-Saclay, 2021.

[3] V. Dos Santos, " Conducted electromagnetic emissions modeling in adjustable speed motor drive systems. Parametric studies and optimization of an inverter and filters under EMC constraints. ". PhD dissertation. Toulouse, INPT, 2019.

[4] T. Hadden et al., "A Review of Shaft Voltages and Bearing Currents in EV and HEV Motors," in IECON 2016 - 42nd Annual Conference of the IEEE Industrial Electronics Society, Oct. 2016, pp. 1578–1583. doi: 10.1109/IECON.2016.7793357.

[5] M. J. Costello, "Shaft voltages and rotating machinery," IEEE Trans. Ind. Appl., vol. 29, no. 2, pp. 419–426, Mar. 1993, doi: 10.1109/28.216553.

[6] T. Plazenet, T. Boileau, C. Caironi, and B. Nahid-Mobarakeh, "A Comprehensive Study on Shaft Voltages and Bearing Currents in Rotating Machines," IEEE Trans. Ind. Appl., vol. 54, no. 4, pp. 3749–3759, Jul. 2018, doi: 10.1109/TIA.2018.2818663.

[7] M. Asefi and J. Nazarzadeh, "Survey on high-frequency models of PWM electric drives for shaft voltage and bearing current analysis," IET Electr. Syst. Transp., vol. 7, no. 3, pp. 179–189, Sep. 2017, doi: 10.1049/iet-est.2016.0051.

[8] U. T. Shami and H. Akagi, "Identification and Discussion of the Origin of a Shaft End-to-End Voltage in an Inverter-Driven Motor," IEEE Trans. Power Electron., vol. 25, no. 6, pp. 1615–1625, Jun. 2010, doi: 10.1109/TPEL.2009.2039582.

[9] Morgan, D., and B. Mulhall. "A Handbook for EMC Testing and Measurement." Measurement Science and Technology 6.5 (1995): 600.

[10] Mariscotti, Andrea, and Leonardo Sandrolini. "Review of models and measurement methods for compliance of electromagnetic emissions of electric machines and drives." *ACTA IMEKO* (2021).

[11] D. Zhao, K. Shen, W. Liu, L. Lang and P. Liang, "A Measurement-Based Wide-Frequency Model for Aircraft Wound-Rotor Synchronous Machine," in IEEE Transactions on Magnetics, vol. 55, no. 7, pp. 1-8, July 2019, Art no. 8105408, doi: 10.1109/TMAG.2019.2900616.

[12] Kohji Maki, Hiroki Funato and Liang Shao, "Motor modeling for EMC simulation by 3-D electromagnetic field analysis," 2009 IEEE International Electric Machines and Drives Conference, 2009, pp. 103-108, doi: 10.1109/IEMDC.2009.5075190.

[13] M. A. Gries and B. Mirafzal, "Permanent Magnet Motor-Drive Frequency Response Characterization for Transient Phenomena and Conducted EMI Analysis," IEEE APEC 2008 (2008) pp.1767-1775.

[14] N. Boucenna, " HF common mode EMC modeling of AC three-phase motors ". PhD dissertation. École normale supérieure de Cachan-ENS Cachan, 20

[15] H. H. Sathler, B. Cougo, J. -P. Carayon, F. Costa and D. Labrousse, "Modeling of Common-Mode Voltage Source for Multilevel Inverter Topologies," *2020 International Symposium on Electromagnetic Compatibility - EMC EUROPE*, Rome, Italy, 2020, pp. 1-3, doi: 10.1109/EMCEUROPE48519.2020.9245681.

[16] U. R. Patel and P. Triverio, "MoM-SO: A Complete Method for Computing the Impedance of Cable Systems Including Skin, Proximity, and Ground Return Effects," in *IEEE Transactions on Power Delivery*, vol. 30, no. 5, pp. 2110-2118, Oct. 2015, doi: 10.1109/TPWRD.2014.2378594.

[17] N. Boucenna, F. Costa, S. Hlioui and B. Revol, "Strategy for Predictive Modeling of the Common-Mode Impedance of the Stator Coils in AC Machines," in IEEE Transactions on Industrial Electronics, vol. 63, no. 12, pp. 7360-7371, Dec. 2016, doi: 10.1109/TIE.2016.2594052.

[18] J. E. Ruiz-Sarrió, F. Chauvicourt, J. Gyselinck and C. Martis, "High-Frequency Modelling of Electrical Machine Windings Using Numerical Methods," 2021 IEEE International Electric Machines & Drives Conference (IEMDC), 2021, pp. 1-7, doi: 10.1109/IEMDC47953.2021.9449561.

[19] Ruiz-Sarrio, Jose E., et al. "Impedance Modelling Oriented Towards the Early Prediction of High-Frequency Response for Permanent Magnet Synchronous Machines." *IEEE Transactions on Industrial Electronics* (2022).

[20] Moreno, Yerai, et al. "Analysis of permanent magnet motors in high frequency—a review." Applied Sciences 11.14 (2021): 6334.

[21] Pastura, Marco & Nuzzo, Stefano & Immovilli, Fabio & Toscani, Andrea & Rumi, Alberto & Cavallini, Andrea & Franceschini, Giovanni & Barater, Davide. (2021). Partial Discharges in Electrical Machines for the More Electric Aircraft—Part I: A Comprehensive Modeling Tool for the Characterization of Electric Drives Based on Fast Switching Semiconductors. IEEE Access. PP. 1-1. 10.1109/ACCESS.2021.3058083.

[22] V. Mihaila, "New conception for AC machine's stator winding minimizing dV/Dt ". PhD dissertation. Artois, 2011.

[23] V. Mihaila, S. Duchesne and D. Roger, "A simulation method to predict the turn-to-turn voltage spikes in a PWM fed motor winding," in *IEEE Transactions on Dielectrics and Electrical Insulation*, vol. 18, no. 5, pp. 1609-1615, October 2011, doi: 10.1109/TDEI.2011.6032831.

[24] A. Hoffmann, B. Knebusch, J. O. Stockbrügger, J. Dittmann and B. Ponick, "High-Frequency Analysis of Electrical Machines Using Probability Density Functions for an Automated Conductor Placement of Random-Wound Windings," *2021 IEEE International Electric Machines & Drives Conference (IEMDC)*, 2021, pp. 1-7, doi: 10.1109/IEMDC47953.2021.9449557.

[25] M. S. C. Pechlivanidou and A. G. Kladas, "Litz Wire Strand Shape Impact Analysis on AC Losses of High-Speed Permanent Magnet

[26] D. Meeker, "Finite element method magnetics," FEMM, vol. 4, p. 161, 2020.

[27] M. D'Antonio, S. Chakraborty and A. Khaligh, "*Planar Transformer With Asymmetric Integrated Leakage Inductance Using Horizontal Air Gap*," in IEEE Transactions on Power Electronics, vol. 36, no. 12, pp. 14014-14028, Dec. 2021, doi: 10.1109/TPEL.2021.3089606.

[28] Saltelli, Andrea, et al. *Global sensitivity analysis: the primer*. John Wiley & Sons, 2008.

[29] Rasmussen, Carl Edward, and Christopher KI Williams. *Gaussian processes for machine learning*. Vol. 1. Cambridge, MA: MIT press, 2006.

[30] Gallard, F., Vanaret, C., Guénot, D, et al. "GEMS: A Python Library for Automation of Multidisciplinary Design Optimization Process Generation". In : 2018 AIAA/ASCE/AHS/ASC Structures, Structural Dynamics, and Materials Conference. 2018. p. 0657.

[31] J. E. Ruiz-Sarrio, F. Chauvicourt and C. Martis, "Sensitivity Analysis of a Numerical High-Frequency Impedance Model for Rotating Electrical Machines," *2022 International Conference on Electrical Machines (ICEM)*, Valencia, Spain, 2022, pp. 1260-1266, doi: 10.1109/ICEM51905.2022.9910666.